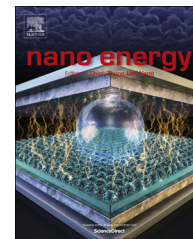Available online at www.sciencedirect.com

ScienceDirect

journal homepage: www.elsevier.com/locate/nanoenergy

ELSEVIER

COMMUNICATION

Nano-heaters: New insights on the outstanding deposition of dielectric energy on perovskite nanoparticles

CrossMark

J. Gracia[c,*], M. Escuin[a], R. Mallada[a,b], N. Navascues[b], J. Santamaria[a,b,]**

[a]Institute of Nanoscience of Aragon, Universidad de Zaragoza, 50018 Zaragoza, Spain
[b]Networking Research Centre CIBER-BBN, 28029 Madrid, Spain
[c]Syngaschem BV, 5600MB Eindhoven, The Netherlands

Abstract
It has been experimentally observed that, in some Mott nanomaterials, outstanding dielectric losses may appear at microwave frequencies, leading to a rapid increase of temperature. This often takes place in association with the insulator to metal transition (IMT) in these materials. However, when other materials with a similar structure and composition are subjected to the same intensity of microwave (MW) irradiation, the observed heating is minimal. Here we show that the electron dynamics of these materials are responsible for their different heating behaviour. More specifically, for $LaCoO_3$ perovskite nanoparticles, the spin shifts causing the IMT are also responsible for the observed heating behaviour. Under suitable conditions, the intense absorption of MW radiation leads to extremely high heating rates, above 600 degrees per second. The insight gained from this study has been used to design a directly heated catalytic system ($LaCoO_3$ perovskite nanoparticles on a MW-transparent cordierite monolith) capable to operate under a stable, significant solid-gas temperature gradient.
© 2015 The Authors. Published by Elsevier Ltd. This is an open access article under the CC BY-NC-ND license (http://creativecommons.org/licenses/by-nc-nd/4.0/).

Introduction

Achieving a highly localized heating (i.e., delivering energy directly and precisely to a region of reduced dimensions) has long been a challenging objective in scientific research. When the dimensions of the desired hot spots are of micron

or sub-micron dimensions, conventional heating mechanisms (conduction and convection) are not able to deliver sufficient spatial precision, and electromagnetic fields capable of selective interactions with certain materials become the only option. Thus, magnetic nanoparticles can be used as targets in the presence of alternating magnetic fields [1] and plasmonic nanoparticles with suitable characteristics are able respond to electromagnetic radiation [2]. Both types of nanoparticles have given rise to a variety of applications demanding localized heating, especially in the biomedical field [3].

On the other hand, microwave heating has been extensively studied as an alternative method to supply energy to a variety of liquid and solid materials. Unlike conventional heating, where conduction and convection are the usual heating mechanisms, microwaves provide energy to susceptible materials in a direct manner, resulting in the volumetric heating of materials capable of dielectric loss. Microwaves (MW) also afford the possibility of selective heating, meaning that a target material can be selectively heated inside a non-absorbing (or comparatively less absorbing) matrix. This characteristic allows the creation of hot spots from which heat is transferred by conduction to a comparatively cooler bulk material, and has been used in applications as diverse as ignition of energetic composites, combustion synthesis of advanced materials, powder sintering, cancer treatment or catalysis [4-9]. Ideally, if a sufficiently intense deposition of energy can be achieved, nanoparticles made of microwave absorbing materials could act as efficient energy sinks, providing a highly localized, nano-sized hot spot.

Achieving this level of enhancement of MW absorption is challenging, not less because the mechanisms of MW heating of solid materials are far from completely understood. Thus, MW heating of a solution containing polar molecules can be reasonably well explained as a consequence of dipole rotations. However in solids, where there are no dipoles able to rotate freely, heating is explained as the result of different categories of polarization induced by the electric field, namely electronic, atomic, dipolar and interfacial polarizations. Even for relatively simple systems, this may lead to an interplay of influences that are not easily visualized in terms of a single physical model. Take as an example amorphous carbon. This is a relatively homogeneous solid where heating is often explained mainly as a result of interfacial polarization (Maxwell- Wagner-Sillars or MWS polarization). However, there are significant reservations regarding the applicability of this model, based on the differences between the basic assumptions of the MWS model and the features of carbon-based solids [10]. If the concentration of impurities or defects is significant, such as in carbon nanotubes, other heating mechanisms and complex interactions have to be taken into account [11], further complicating the understanding and control of the process of energy deposition.

For perovskite materials complexity increases, since a range of stoichiometries and crystal structures are possible (perovskites can accommodate around 90% of the metallic elements of the Periodic Table [12]) which increases the possibilities regarding electronic configurations and their response to coupled external fields. Most perovskites are easily heated by microwaves, but the differences in heating

rates can be very substantial. While the absorption of microwave power (and therefore the heating rate) is usually related to the loss tangent, $\tan \delta = \varepsilon''/\varepsilon'$, defined as the ratio between the dielectric loss and the dielectric constant of the material, the value of $\tan \delta$ has to be measured experimentally for each material and operating conditions. However, this is an empirical measurement, required because a predictive model capable of explaining the interaction of microwave energy with perovskites is still lacking. A variety of factors have been invoked to justify the diverse behaviour concerning the absorption of microwave power by different perovskite materials and their observed heating rates. These include the nature of the central atom and its number of unpaired d-electrons, as well as the particle size and specific surface area [13], the re-orientation of permanent dipole molecules [14] and the presence of defects in the material [15].

On the other hand, strongly correlated materials, and in particular Mott oxides present competing electronic states and, in the region in which several states are nearly degenerate, perturbations such as electromagnetic fields are able to induce dramatic responses [16]. Also, numerous materials with good coupling at microwave frequencies are metal oxides with incompletely filled d- or f-electron shells and narrow energy bands [17]. Many perovskites share these characteristics and therefore, electron dynamics provide a suitable starting point to investigate the interaction of perovskites with microwaves for heating purposes. In this work we have selected a well-known perovskite ($LaCoO_3$) as the basis of our study, and then used density functional theory to understand its electronic dynamics. The insight gained in the elucidation of the resonant behaviour of $LaCoO_3$ under MW radiation allows us to explain the response (or lack of thereof) of other perovskites to MW fields.

Materials and methods

The different perovskites used in this work were prepared by the citrate method. Initially the desired weights of the corresponding nitrates were dissolved in deionized water. After titration, the solutions were mixed in the desired proportions and N moles of citric acid were added (N being equal to the total number of moles of metals). The solution was maintained at 373 K for 12 h, which rendered a porous gel. This was then ground and calcined in two stages at a rate of 2 K/min, first at 573 K for 30 min, and then at 1073 K for 2 h. The morphology of the samples was observed by scanning electron microscopy (FEI, Inspect F50) and the composition of the samples was analized via Energy Dispersive X-ray (EDX) Spectroscopy. X-ray diffraction (XRD) was used to check the crystal phases present in the synthesized samples using a diffractometer (D-Max Rigaku) using a graphite monochromator for selecting the CuKα radiation (Figure S1, supplementary information). BET specific surface areas were measured by nitrogen adsorption at 77 K (Micromeritics TriStar) and values ranged from 9 to 13 m^2/g for the different perovskites.

The experimental microwave heating system and details of the reactor set up are presented in the supplementary information section (Figure S2, supplementary information).

Of especial interest was set up used for temperature measurements under reaction, which was specifically developed for this work in order to obtain direct temperature readings from the solid surface. All the heating experiments were conducted in ambient air, except the n-hexane combustion experiments, that were performed with a feed containing 200 ppmV n-hexane in air at atmospheric pressure.

Density Functional Theory (DFT) calculations were performed using VASP, Vienna Ab-initio Simulation Package, the details about these calculations are presented in the supplementary information section.

Results and Discussion

Widely different heating behaviour of perovskites under MW irradiation

$LaCrO_3$, $LaMnO_3$, $LaFeO_3$, $LaCoO_3$ and $LaNiO_3$ perovskites (formally d^3 to d^7) have been prepared as nanoparticles with a diameter around 100 nm and then either deposited on MW-transparent cordierite monoliths or pressed into slabs using MW-transparent KBr as binder. The varied (and sometimes counter-intuitive) responses of 200 mg slabs containing respectively 2 and 20 wt% of sensitive material when MW-irradiated at 60 W are shown in Figure 1. It can be seen that the slab with 2 wt% of $LaCoO_3$ heats slowly at first, then the heating rate increases exponentially, reaching 1000 K after 100 seconds. This is in sharp contrast with the observed behaviour for other samples with 2% of perovskite (B=Cr, Fe, Ni, Mn), whose temperature barely increased. For comparison, the results obtained with slabs containing 2% of carbon nanotubes are also shown. In this case a fast ignition in the first few seconds is observed, followed by a slower increase to ca. 723 K. The immediate ignition displayed by CNTs differs from the progressive heating profile of $LaCoO_3$, where abrupt energy absorption occurs only above 473 K. Interestingly in this case, when the concentration of microwave-absorbing material ($LaCoO_3$) was increased by an order of magnitude (from 2 to 20%), a different heating pattern was obtained, and the temperatures reached were lower, with a maximum steady temperature around 730 K (Figure 1B). It should be noticed that of all the slabs with 20% perovskite in Figure 1B, only those structures that may present an uneven occupation of the d orbitals, $LaMnO_3$, $LaCoO_3$ and $LaNiO_3$, heat up significantly (Table 1). In addition, their heating pattern is similar to that observed for the 2% CNT sample: immediate ignition followed by a levelling off of the temperature curve. On the other hand, $LaCrO_3$ and $LaFeO_3$ without unpaired e_g electrons, showed a negligible increment of the temperature, even at 20% loading.

This heating behaviour can be rationalized by noting that $LaNiO_3$ is metallic in all the temperature range while $LaCoO_3$ and $LaMnO_3$ start metallic transitions around 500 K and 750 K respectively. A perovskite loading of 20% is above the percolation threshold of the slabs, and therefore the samples will present a metal-like behaviour after the insulator-metal transition (IMT), reflecting most of the radiation. As a consequence, after a fast initial ignition, the temperature levels off (Figure 1B). It is interesting to note that this is the same behaviour observed for CNTs. In
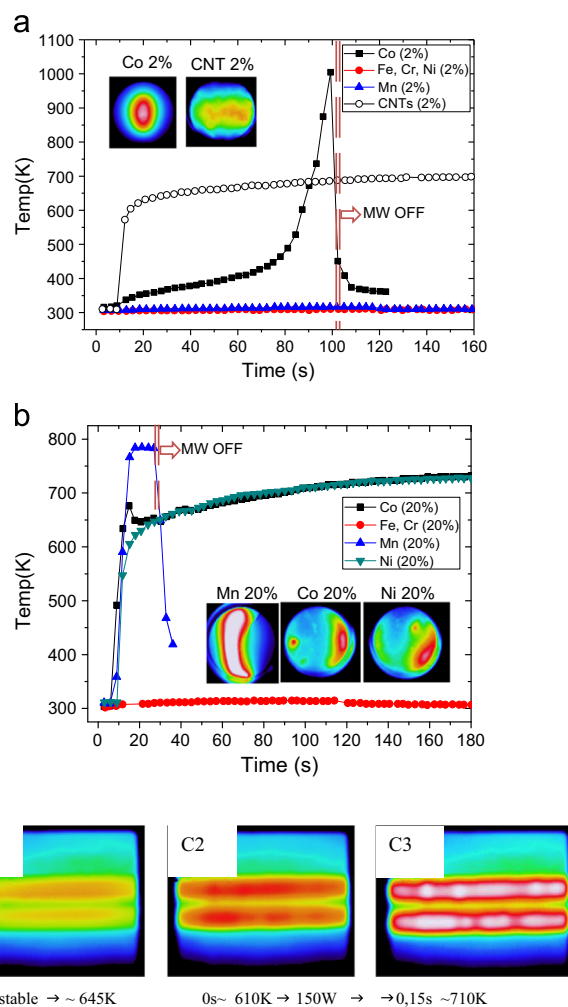

65W stable → ~645K   0s~ 610K → 150W →   →0,15s ~710K

Figure 1 (A) Heating curves at 60W of 200 mg slabs containing 2% of $LaBO_3$ (B = Cr, Mn, Fe, Co, Ni) perovskite or CNTs and 98% KBr as agglutinant. B) Samples with 20 % of perovskites and 80% KBr. The insets in A) and B) correspond to thermal images of the spherical slabs containing the MW-sensitive materials. C) A flash heating experiment with 0.18 mg of $LaCoO_3$ deposited on MW-transparent quartz channels. C1: The sample is stabilized under 65 Watts at ~645 K. C2) Power is switched off and sample allowed to cool to ~610 K. C3) Power on again. After 0.15 s at 150 W 710 K are reached (see video in Electr. Supp. Information).

this case, due to their extremely high aspect ratio, percolation can be achieved with low loads and a 2 wt% nanotube content is already above the threshold. In contrast, a 2 wt% perovskite load is not enough to make the slabs conductive, and the $LaCoO_3$ nanoparticles display the maximum dielectric loss. An inflection in the heating curve can be seen close to 500 K indicating the progressive IMT that takes place in the nanoparticles. To have a direct illustration of the extremely fast MW absorption of this perovskite above the IMT, a small amount of $LaCoO_3$ nanoparticles was deposited on MW-transparent quartz grooves (Figure 1C). The sample temperature was carefully stabilized at 645 K, well above the IMT value, then allowed to cool slightly to 610 K and subjected to a power of 150 W. The fast MW absorption led

Table 1 Electronic configuration, magnetic behaviour and energy gap for the perovskites tested in this work.
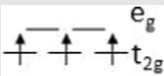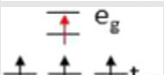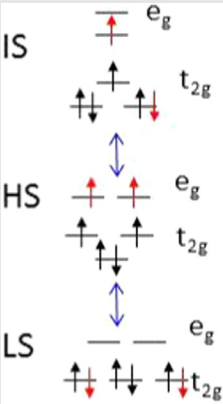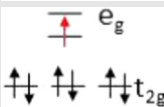
Perovskite	Electronic Configuration	Magnetic properties	Electrical properties
LaCrO$_3$		Antiferromagnetic (T$_{Neel}\sim$300K)	Insulator Optical gap $\sim$4eV
LaMnO$_3$		Antiferromagnetic (T$_{Neel}\sim$140K)	Semiconductor Optical gap $\sim$1,2eV IMT transition at 750K
LaFeO$_3$		Antiferromagnetic (T$_{Neel}\sim$740K)	Insulator Optical gap $\sim$2,2eV
LaCoO$_3$		Diamagnetic Transition at T=80K to Paramagnetic	Semiconductor Optical gap $<$1,2eV IMT transition at 500K
LaNiO$_3$		Paramagnetic	Metallic

Table 2 DFT Co-O distances (Å) for different values of the GGA+U approach versus experimental determinations for LaCoO$_3$ (I2/a).

Ordering	Spin	LaCoO$_3$ I2/a	Co-O$_1$ (Å)	Co-O$_2$ (Å)	Co-O$_3$ (Å)	ΔE(eV)
		Experimental (250 K)	1.877	1.935	1.979	
FM	LS	U=4	1.910	1.910	1.910	
FM	HS	U=7.6	1.866	1.952	1.974	
FM	HS	U=7.8	1.864	1.951	1.974	
FM	HS	U = 8	1.862	1.949	1.970	0.94
AF	HS	U=8	1.863	1.944	1.955	0.00
FM	IS	U=8	1.928	1.928	1.930	1.05
FM	HS	U=8.2	1.859	1.948	1.972	

to heating rates exceeding 600 K/s (*see video in support online material*).

Supplementary material related to this article can be found online at http://dx.doi.org/10.1016/j.nanoen.2015.11.040.

Theoretical Calculations

Many transition metal oxides show an insulating Mott phase in which holes and occupied sites form bound states due to their coulomb interactions [18]. The universal energy gaps exhibited by nominally metallic carbon-nanotubes also agree with a Mott state [19]. It is also well established that temperature, pressure, doping, magnetic fields and electric fields can trigger various types of metal-insulator transitions in transition metal oxides [20]. Because of the perturbations, the localized electron character progresses gradually towards a collective model. However, the emerging conducting state from the IMT differs considerably from that corresponding to free electrons in conventional metals [21], since the displacement of atoms is required to allow the movement of the charge carriers (polarons). Accordingly the effective mass for the vibronic charge carrier is generally greater than that of a free electron. Polarons are very slow compared with the electronic oscillations in typical metals

and the relaxation rates of the polarons fall into the microwave regime [22]. This means that it is possible to induce collective oscillations of the polarons in resonance at microwave frequencies.

In its ground state LaCoO$_3$ is a diamagnetic insulator, as the temperature is raised to $\sim$90 K, it becomes paramagnetic, and with a further increase to $\sim$500 K the IMT takes place. The competition between low-spin (LS)$t_{2g}^6 e_g^0$, high-spin (HS)$t_{2g}^4 e_g^2$, and intermediate-spin (IS)$t_{2g}^5 e_g^1$ states for Co^{3+} atoms accounts for the observed changes in the properties for rare-earth cobaltites. The low spin $t_{2g}^6 e_g^0$ configuration is predominant at the lowest temperatures. The thermal population of the high-spin state confirms the first state crossover at $\sim$90 K (LS-HS) [23,24]. With increasing temperature, at around 500 K, a gradual insulator-metal crossover starts that shows the characteristics of a Mott transition in strongly correlated electron systems [25]. Our calculations indicate that the semiconductor to metal transition in LaCoO$_3$ proceeds via intermediate spin (IS)$t_{2g}^5 e_g^1$ mixed states (Table 3). The HS state is more stable than IS [26] and the IS state has a metallic band structure [24], likely to organize in a ferromagnetic exchange interaction [25].

Our calculations for HS Cobalt agree well with published X-ray diffraction data [26] in showing the presence of a coherent Jahn-Teller effect with three unequal Co-O bond lengths: one short ($\sim$1.87 Å), one long ($\sim$1.97 Å) and one medium ($\sim$1.95 Å). The Jahn-Teller distortion of each Cobalt atom prevails in mixed conformations (HS-IS) with metal atoms in different spin states. Due to the increasing electron delocation the degeneracy of the e_g orbitals recovers for the final metallic ferromagnetic phase with all the Cobalt atoms in the IS state (Table 2).

The dielectric loss in perovskites has an origin associated to electronic relaxation mechanisms. Ab-initio calculations allow us to identify the local shifts of the LaCoO$_3$ electron density due to the $t_{2g}^4 e_g^2$ to $t_{2g}^5 e_g^1$ spin crossover in the Co atoms. A net charge transfers from the oxygen atoms to the central Cobalt, see Figure 2. The e orbital has a Co-O antibonding character versus the nonbonding t orbital; Co atoms reduce by $\sim$0.2 electrons after the HS$\rightarrow$IS inversion. Such process constitutes a dielectric relaxation mechanism with a natural resonance frequency that depends on the activation energy required for the orbital transition. We observe the pronounced decrease of the activation energy for the HS$\rightarrow$IS spin crossover with the development of ferromagnetic ordering (Figure 2 and Table 3). At the IMT, the orbital excitation ($e \rightarrow t$) becomes an effective dielectric relaxation mechanism related to the lifetime of the charge carriers. Because the spin gap progressively diminishes, LaCoO$_3$ evolves towards collective electron oscillations with an intrinsic relaxation mechanism that gradually enters in resonance with the MW field.

At the spin-crossover, the lattice polarization adapts to the charge distribution of the diverse electronic configurations, a dynamic process that involves continuous shifting of the wave function according to the changing electromagnetic field. The radiated energy is primarily dropped to the resonant collective oscillations of the charge carriers, and the electrons transfer their energy to the lattice through the modification of the Jahn-Teller distortions associated with the dielectric relaxation mechanism. This kind of
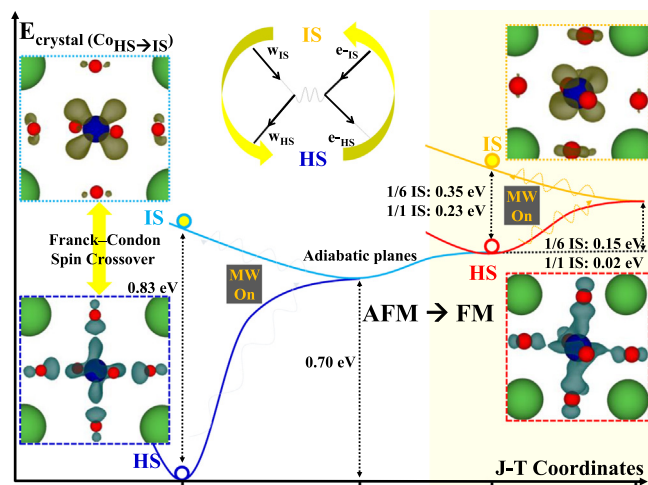

Figure 2 Energy diagram and calculated charge transfer in LaCoO3 due to the HS to IS orbital excitation in Co atoms.

thermal process takes several picoseconds [27], orders of magnitude faster than the oscillation of the excitation in our study. Therefore, equilibrium thermodynamics predominantly account for experimental data [28]. As shown in Figure 1, the continuous conversion of microwave energy into heat through the electron-phonon coupling raises the temperature of the LaCoO$_3$ sample, first gradually, then exponentially, as the oscillations of the charge carriers couple to the external MW field around the IMT.

Application to direct catalyst heating

A nanosized hot spot can find application in a multitude of scenarios, as explained in the Introduction. However, since perovskites are active oxidation catalysts themselves, we have chosen as a proof of concept, a combustion reaction (n-hexane in air) application, where the perovskite catalyst is selectively heated. Given the difficulties involved in measuring temperatures in closed systems (chemical reactors) under MW heating (see for instance [29]) we have developed a specific design in which the MW-transparent cordierite monolith with the dispersed perovskite nanoparticles (Figure 3) has been housed in a quartz reactor with a ZnSe window that allows direct observation of the cordierite monolith using a thermographic camera, while an IR optical fiber in contact with the outer (downstream) surface of the monolith, measured the temperature of the gases exiting the reactor (see supplementary information for details of the set up). The same set up was used under conventional (electrical) heating to compare the reactor performance under both heating modes.

As expected, with a perovskite loading around 5 wt%, well dispersed on the cordierite monolith (Figure 3, middle), the LaCoO$_3$ perovskite heated efficiently under a MW power of 30 W, while under the same conditions a very small temperature increase was measured for the LaMnO$_3$ sample (Figure 3, top). To check the stability of the LaCoO$_3$ perovskite under MW heating a series of 10 MW heating cycles were performed during which temperatures higher than 623 K were reached. A detailed comparison of the XRD results obtained before and after the heating experiments

Table 3 DFT (U = 8) predictions for different LaCoO$_3$ spin states, C1[R3-c] unit cell.

|	Spin Ordering	Co Electronic State	ΔE (eV)	Co$_{Charge}$ (e⁻)		Co$_{Magnetic\ Moment}$ (e⁻$_{up}$- e⁻$_{down}$)	
				HS	IS	HS	IS
A	AF	$t_{2g}^4 e_g^2$ (HS)	0.00	1.71		±3.1	
B	AF	1/6 $t_{2g}^5 e_g^1$ + 5/6 $t_{2g}^4 e_g^2$	0.70	1.71	1.52	±3.1	-1.9
C	AF	1/3 $t_{2g}^5 e_g^1$ + 2/3 $t_{2g}^4 e_g^2$	1.36	1.71	1.52	±3.1	-1.9
D	AF	1/2 $t_{2g}^5 e_g^1$ + 1/2 $t_{2g}^4 e_g^2$	2.03	1.71	1.52	+3.1	-1.9
E	FM	$t_{2g}^4 e_g^2$	1.40	1.76		+3.2	
F	FM	1/6 $t_{2g}^5 e_g^1$ + 5/6 $t_{2g}^4 e_g^2$	1.55	1.75	1.50	+3.1	+2.7
G	FM	1/3 $t_{2g}^5 e_g^1$ + 2/3 $t_{2g}^4 e_g^2$	1.67	1.75	1.49		
H	FM	1/2 $t_{2g}^5 e_g^1$ + 1/2 $t_{2g}^4 e_g^2$	1.86	1.73	1.50	+2.9	+2.5
I	FM	$t_{2g}^5 e_g^1$ (IS)	1.88		1.47		+2.4
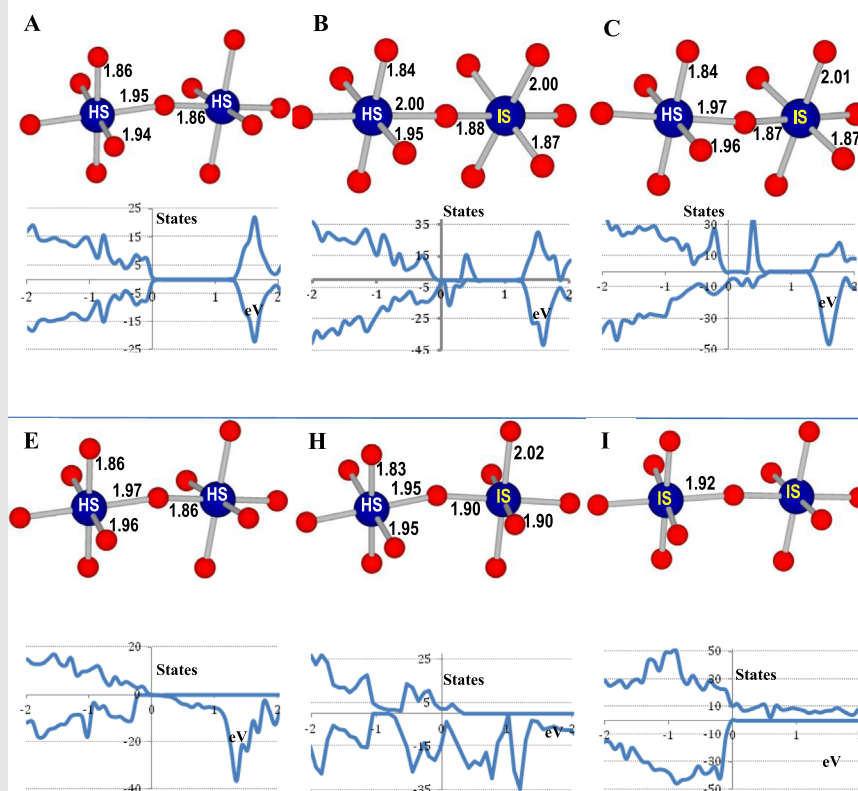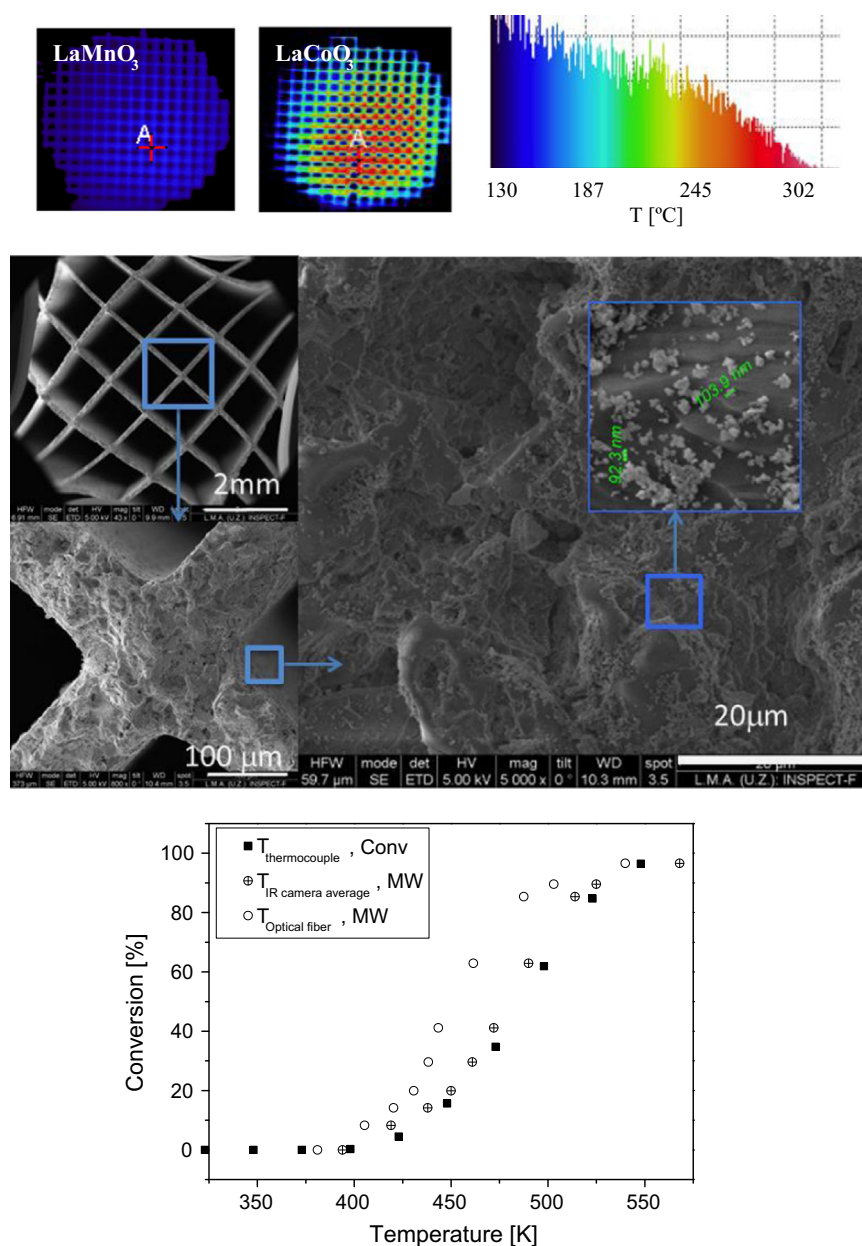
Figure 3 Top. Left: Thermographic IR images of the LaMnO₃ and LaCoO₃-coated cordierite monoliths under microwave irradiation. Right: Temperature distribution obtained from a thermographic image of the LaCoO₃-coated cordierite monolith, from which the average surface temperature can be calculated. Middle: Scanning Electron Microscopy views of the surface of the cordierite monolith after coating with LaCoO₃ nanoparticles. Magnification increases anticlockwise from the upper left hand corner. Bottom: Light-off curves obtained under conventional (□) and microwave heating (crossed circles: average solid temperature measured by an Infrared Camera and open circles: exit gas temperature measured by an Optical Fiber) for Hexane combustion with (~36 mg) of LaCoO₃ nanoparticles on a cordierite monolith (200 ppm in air 4 ml/min · mg).

(Figure S3, supplementary information) showed no differences in the XRD patterns regarding the peak positions or the crystallite size, calculated from the Scherrer equation (around 15 nm in both cases).

The results of the reaction experiments (Figure 3, bottom) show that the same light-off curve is obtained irrespective of the heating mechanism (MW heating or conventional heating) provided that the average monolith temperature (IR camera, MW heating) and the temperature measured with a thermocouple in the middle of the monolith (conventional heating) are used as references. However,

under MW heating the temperature measured by the IR probe was considerably lower (~40 K) than the average temperature obtained with the thermographic IR camera. This reflects different heating dynamics: MW radiation selectively heats perovskite nanoparticles while the cordierite support and the gas phase are largely microwave-transparent. The cordierite monolith heats rapidly by conduction from the perovskite nanoparticles, and releases heat towards the gas phase. As a consequence, a significant temperature difference can be established between the directly heated catalytic monolith and the relatively colder

gas stream in the reactor. This is in contrast with conventional heating, where the catalyst is heated by conduction through the reactor wall and convection from the gas phase, and the gas-solid temperature gradient is minimal. Thus, by using simultaneously perovskite nanoparticles as MW susceptors and catalysts, the energy lost in the gas stream is lowered, and a higher energy efficiency can be obtained.

Conclusions

The above results demonstrate the central role of the high spin (HS) to intermediate spin (IS) crossover in LaCoO$_3$-based perovskites to account for their heating under MW radiation. The process leads to highly localized heating, with the initial formation of hot spots of nanosized dimensions. Not completely unlike the photothermal effects that result in the heating of plasmonic nanoparticles by NIR radiation, here electron movements are also responsible for the deposition of electromagnetic energy. However, the use of Mott materials such as the LaCoO$_3$ perovskites investigated in this work widens considerably the applicable wavelengths, to include microwave and radiofrequency. As a proof of concept, microwave irradiation has been used to deliver energy to catalytic perovskite nanoparticles dispersed on a MW-transparent cordierite support. This resulted in a significant temperature gap between the solid surface and the bulk gas phase, paving the way for substantial energy savings.

The concept of MW-localized heating can be applied to other nanoscale Mott materials such as those based on carbon (carbon nanotubes, graphene, fullerenes), metallic oxides (Vanadium, Cobalt or Nickel oxides), and other perovskites. The Mott material and the support must be selected according to the specific application and the range of temperatures of interest.

Acknowledgements

Appendix A.   Supplementary material

Supplementary data associated with this article can be found in the online version at http://dx.doi.org/10.1016/j.nanoen.2015.11.040.

References

[1] A.E. Deatsch, B.A. Evans, J. Magn. Magn. Mater. 354 (2014) 163-172.
[2] A.O. Govovov, H.H. Richardson, Nano Today 2 (2007) 30-38.
[3] B.E. Smith, P.B. Roder, X.Z. Zhou, P.J. Pauzauskie, Nanoscale 7 (2015) 7115-7126.
[4] C.A. Crane, M.L. Pantova, B.L. Weeks, J. Appl. Phys. 115 (2014) 104106.
[5] R. Rosa, P. Veronesi, C. Leonelli, G. Poli, A. Casagrande, Surf. Coat. Technol. 232 (2013) 666-673.
[6] R. Heuguet, S. Marinel, A. Thuault, A. Badev, J. Am. Ceram. Soc. 96 (2013) 3728-3736.
[7] H. Shi, T. Liu, C. Fu, L. Li, L. Tan, J. Wang, X. Ren, J. Ren, J. Wang, X. Meng, Biomaterials 44 (2015) 91-102.
[8] L. Bo, J. Liao, Y. Zhang, X. Wang, Q. Yang, Front. Environ. Sci. Eng. 7 (2013) 395-402.
[9] T. Durka, T. Van Gerven, A. Stankiewicz, Chem. Eng. Technol. 32 (2009) 1301-1312.
[10] T. Kim, J. Lee, K.H. Lee, Carbon Lett. 15 (2014) 15-24.
[11] E. Vazquez, M. Prato, ACS Nano 3 (2009) 3819-3824.
[12] J. Zhu, H. Li, L. Zhong, P. Xiao, X. Xu, X. Yang, Z. Zhao, J. Li, ACS Catal. 4 (2014) 2197-40.
[13] T. Krech, C. Möser, R. Emmerich, P. Scholz, B. Ondruschka, J. Cihlar, Chem. Eng. Technol. 31 (2008) 1000-1006.
[14] Y. Zhang-Steenwinkel, H.L. Castricum, A. Bliek, E. Esveld, J. Mater. Sci. 42 (2007) 5851-5859.
[15] T. Krech, R. Krippendorf, B. Jäger, M. Präger, P. Scholz, B. Ondruschka, Chem. Eng. Proccess 71 (2013) 3136.
[16] E. Dagotto, Science 309 (2005) 257-262.
[17] E. Reguera, C. Diaz-Aguila, H. Yee-Madeira, J. Mater. Sci. 40 (2005) 5331-5334.
[18] P. Limelette, A. Georges, D. Jerome, P. Wzietek, P. Metcalf, J.M. Honig, Science 302 (2003) 89-92.
[19] V.V. Deshpande, B. Chandra, R. Caldwell, D.S. Novikov, J. Hone, M. Bockrath, Science 323 (2009) 106-110.
[20] J.S. Brockman, L. Gao, B. Hughes, C.T. Rettner, M.G. Samant, K.P. Roche, S.S.P. Parkin, Nat. Nanotech. 9 (2014) 453-458.
[21] M.M. Qazilbash, M. Brehm, B.-G. Chae, P.C. Ho, G.O. Andreev, B.-J. Kim, S.J. Yun, A.V. Balatsky, M.B. Maple, F. Keilmann, H.-T. Kim, D.N. Basov, Science 318 (2007) 1750-1753.
[22] D.N. Basov, R.D. Averitt, D. van der Marel, M. Dressel, K. Haule, Rev. Mod. Phys. 83 (2011) 471-541.
[23] M.J.R. Hoch, S. Nellutla, J. van Tol, E.S. Choi, J. Lu, H. Zheng, J.F. Mitchell, Phys. Rev. B 79 (2009) 214421-214427 214421-1.
[24] H. Hsu, P. Blaha, R.M. Wentzcovitch, C. Leighton, Phys. Rev. B 82 (2010).
[25] Y. Tokura, Y. Okimoto, S. Yamaguchi, H. Taniguchi, T. Kimura, H. Takagi, Phys. Rev. B 58 (1998) R1699-R1702.
[26] S. Mukhopadhyay, M.W. Finnis, N.M. Harrison, Phys. Rev. B 87 (2013) 125132-125139 224423-1-.
[27] M. Liu, H.Y. Hwang, H. Tao, A.C. Strikwerda, K. Fan, G.R. Keiser, A.J. Sternbach, K.G. West, S. Kittiwatanakul, J. Lu, S.A. Wolf, F.G. Omenetto, X. Zhang, K.A. Nelson, R.D. Averitt, Nature 487 (2012) 345-348.
[28] S.K. Sundaram, E. Mazur, Nat. Mater. 1 (2002) 217-224.
[29] T. Durka, G.D. Stefanidis, T. Van Gerven, A. Stankiewicz, Meas. Sci. Technol. 21 (2010) 45108.
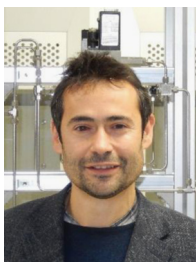
Jesus Santamaria received his PhD in Chemical Engineering from the University of Salford, UK and has done postdoctoral stays at Notre Dame University and MIT (USA). He became a Professor of Chemical Engineering at the University of Zaragoza, where he is vice-Director of the Nanoscience Institute of Aragon and holds the SAMCA chair in Nanotechnology. Since 2000 he has been one of the Editors of the Chemical Engineering Journal. His research addresses the preparation of nanomaterials and the development of applications in a variety of fields: microreactors, nano-assisted theraphy, catalytic reactors capable of non-conventional heating, nano-structured chemical sensors and nanosafety.

Reyes Mallada is Associate Professor in the Chemical and Environmental Engineering Department since 2007 and member of the Institute of Nanoscience of Aragon since its creation in 2003. Her experience in materials science, nanomaterials, catalysis, membranes and reaction engineering is reflected on more than 50 papers. She is currently working on catalyst activation by diffeent energy forms including microwaves and light, catalytic microreactors, nanostructured membranes and membrane based microdevices.

Nuria Navascués received her Bachelor degree of science in Chemistry. She obtained her PhD from Zaragoza University in 2008. During this time, her research focused on the synthesis and characterization of tailored porous material with controllable adsorption properties. Since 2008, she has worked at Institute of Nanoscience of Aragon (INA, Zaragoza University). Her research interest involve development of catalyst for heterogeneous reaction (VOC oxidation, CO selox) heated by conventional or microwave heating, as well as improvement in the properties of polymer nanocomposites.
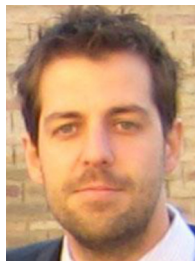
Jose Gracia is Deputy Director Research at Syncat@Beijing, the Institute for fundamental catalysis research of Synfuels China Technology Co., Ltd. He received his PhD in Theoretical Chemistry from the Rovira i Virgili University of Tarragona (2004). Since then he specialized in computational chemistry to understand physico-chemical processes in various international academic and industrial projects. The last eight years he focused on heterogeneous catalysis at the universities of Eindhoven and Zaragoza, and at Syngaschem BV, Eindhoven; he joined Synfuels China in May 2015. His research interests are surface chemistry, materials science and energy efficiency.

Miguel Escuin obtained his Bachelor degree in chemistry and a Master degree in chemical engineering at the university of Zaragoza where he is currently a PhD student. He has worked for 6 years at the Nanoscience Institute of Aragon on projects using heterogeneous catalysis to remove air pollutants using nanoporous materials like zeolites. His current research is aimed to find catalysts capable of efficiently absorbing microwave energy to obtain improvements in the energy efficiency of chemical processes.